ISSN : 0974 - 7443 Volume 10 Issue 1
CHEMICAL TECHNOLOGY
An Indian Journal
Full Paper
CTAIJ 10(1) 2015 [018-032]

Local and global measurements in trickle bed reactor, Part 2: Void fraction and film thickness

Shripad T.Revankar[1,2]*, Xiangcheng Kong[1]
[1]School of Nuclear Engineering, Purdue University, West Lafayette, IN 47907, (USA)
[2]Division of Advanced Nuclear Engineering, POSTECH, Pohang, Gyeongbuk 790-784, Republic of Korea, (KOREA)
E-mail : shripad@purdue.edu; shripad@postech.ac.kr

ABSTRACT

In this paper two phase air water flow parameters in trickle bed reactors were measured using impedance void meter and film thickness probes to characterize the two phase flow behaviour and structure both at bed level and at pore level. The data on the gas phase void fraction, liquid hold up and pulse velocity were obtained for various flow rates of gas and liquid. The signals for the impedance meter and the film thickness probe provided the wave nature of liquid film and its impact on the void fraction and liquid holdup in the bed. Analysis of the data in terms of FFT and PDF provided signature of flow regimes and characteristics of pulses in pulse flow regime.

KEYWORDS

Trickle bed reactor;
Packed bed air-water flow;
Void fraction;
Film thickness;
Pulse velocity.

INTRODUCTION

Trickle-bed reactors are one of the oldest and most widely used types of catalytic chemical reactors and are used for both single phase and multiphase catalytic reactions especially in petroleum and petrochemical industries[1,2]. There is tremendous interest on how well trickle-bed reactors operate because they have large economic impact. For example, in the petroleum sector alone the annual processing capacity for various hydrotreatments such as hydrodesulfurization, hydrocracking, hydrodemetallization, is in the neighbour of 1.6 billion metric tons. The hydrodynamic (bed pressure drop, liquid hold up) and transport properties (heat and mass transfer) of the trickle bed are dependent on the two phase flow structure and interaction between the two fluids and the solid catalytic packing. Due to these interaction various flow regimes are formed such trickle, pulse, bubbly and spray depending on the fluid flow rates. An understanding of the conditions at which transition from one regime to another occurs, as well as the two-phase flow parameters in each of these regimes, is of fundamental importance in the design and scale-up of these reactors. In view of this, an experimental study is performed in trickle bed reactor with detailed local and global instrumentation to obtain data on void fraction, liquid hold up and pulse velocity.

This paper is second part of two parts series and presents experimental results on pore level measurement of film thickness and bed cross sectional averaged void fraction. Part one paper presents the detail on experiments and measurement of single and two phase pressure drops and flow regime maps.

TWO PHASE FLOW INSTRUMENTATION

One of the main goals of the experiments was to measure pore level two-phase parameters. Considerable effort was put in developing pore level instrumentation for measurement of flow regime transition, void distribution, and pulse velocity, in the trickle bed. Three kinds of instrument were developed which would provide detailed local and global measurement on the two phase flow behaviour in the bed. Film thickness probe is a pore level instruments, while impedance meter provides bed level information. The details on the impedance meter are given in Part 1of the paper.

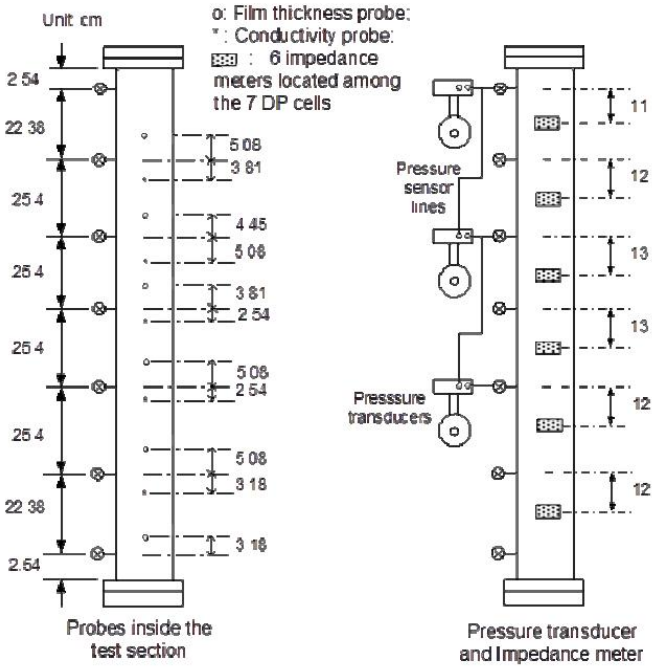

Figure 1 : Instruments and their locations

The instrument locations are shown in Figure 1. The probes, meters, and transducers are numbered from inlet to outlet. Sometimes abbreviations of the names are used in result display. For example, the highest parallel wire film thickness probe is 'PWFP #1'; the lowest impedance meter is 'IM #6'.

Film thickness probe

There are four methods that are generally used for film thickness measurement. These are: (i) Laser reflection method: In this method a CCD camera sensitive to laser takes pictures of cross section of the liquid film. By sending the laser beam on the liquid film produces fringes. The distance between intensity peaks is the measure of the film thickness. (ii) LFD method: Light Confocal Displacement Meter can give a resolution of 1μm. It uses the light refraction principle of liquid. (iii) Capacitance method: This method makes use of the principle that the capacitance between the electrodes is related to the film thickness. (iv) Conductance method: Use the basic relationship between the film thickness the electrical resistance between two electrodes[3].

Conductance probe is defined as the arrangement of two electrodes, in a conducting liquid, excited by a circuit. The film thickness bridging the probes defines the signal output. Three probe configurations have been used for film thickness measurement. They are needle probes, parallel wires and flush mounted pins.

Needle probe

This method relies on the contact made between an electrode mounted flush with the pipe surface and the tip of a needle which could be moved across the liquid film up to the fixed electrode[4]. When the tip of the needle is at or below the gas–liquid interface, a current will flow. As the film is wavy the needle tip will be in the water intermittently. The statistical description of film thickness is built up by positioning the needle tip at a series of distances from the wall and determining the fraction of time that the circuit is completed. The advantage of this method is that it is very precise, does not require calibration and is applicable to a wide range of thickness. Furthermore, it is a much localized measurement. On the other hand, it can be quite intrusive for thin films and it is particularly laborious to operate.

Parallel wires

In this approach, the electrodes are two parallel thin wires[4-7]. These are protruding from the wall where they are supported. As the film thickness increases, the surface area of electrode increases and the resistance decreases. The output depends on the geometric dimensions and on the conductivity of the liquid. It is less reliable for thin films because of its intrusive nature, i.e., the formation of a meniscus due to surface tension effects.

Full Paper

Flush mounted pins

The method is used for very thin films, typically smaller than 2 mm. Electrodes are pins mounted flush with the wall surface and linked to a circuit. The method is non-intrusive but the response is non-linear. The range of film thickness that can be handled depends on the size and spacing of the electrodes. The shorter the spacing, the less the range and the more sensitive is the probe. Design is based on a compromise between the range of operability and local character of the measurement. A composite type, a combination of the flush mounted and a needle probe was used by Kim and Kang[8].

The parallel wire probe is used for the current application to spherical beads. Two wires are mounted on an acrylic bead. The distance between the two electrodes is kept below 2 mm to get linear output. Koskie et al.,[7] showed that the parallel wire probe has high resolution and excellent linearity for various film thicknesses but comparably low sensitivity for thin film thickness. A high frequency based circuit was developed for the measurement of the impedance of the liquid film using the parallel wire probes. When the frequency of the applied voltage, which is called carrier signal, is high enough, the probe impedance is entirely resistive and the capacitance effect is negligible. When a high frequency AC voltage is supplied to one of the two wires, the signal is conducted through the liquid to the second wire, where a custom designed amplifier/converter circuit measures the conducting current which is directly proportional to liquid layer thickness. The circuit is also used to eliminate noise and minimize effects due to leakage currents and interference between probes. A high frequency (100 KHz) voltage from function generator is used as the input to the circuit while DC voltage as the output gives the measure of the film thickness.

The probe as installed on spherical bead and it dimensions are shown in Figure 2. The probe assembly was made the following way. Two precision holes of diameter 343μm separated by distance of 1.016 mm were made on the acrylic bead. Stainless steel tubes of diameter 330 μm were used as probe electrodes. The electrodes were inserted into

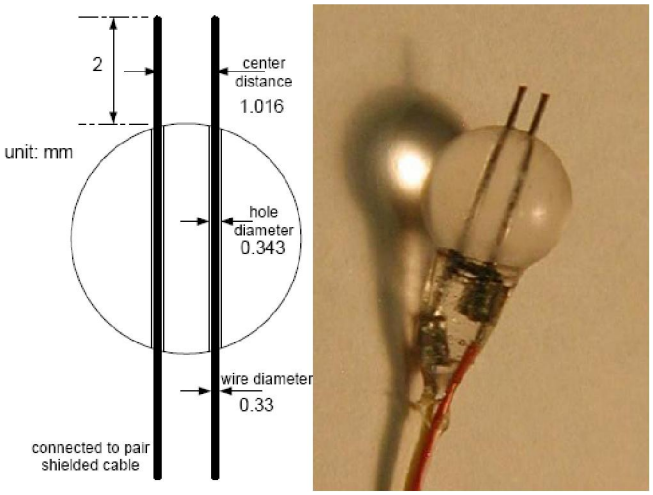

Figure 2 : Dimensions of parallel wire film thickness probe and picture of probe installed on an acrylic bead.

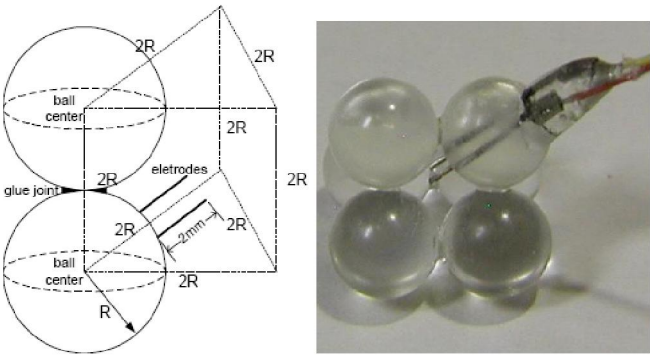

Figure 3 : Structure of a cluster of beads with film thickness probe

the hole and cemented. The height of the probe is 2 mm measured from bead surface to the tip of the probe wire. The other side of the electrodes was connected with extension cable. The distance between the probes wire is 1.016 mm.

In order for the probe to be installed in the bed a cluster of beads was designed so that the probe electrodes are located in one pore volume. This also protects the probe electrodes. The design of the cluster was based on the required porosity of the bed. The test bed porosity with random packing was 0.377. The porosity for the body centre arrangement is 0.320 and that for the cubic centre is 0.477. The equal side prism structure shown in Figure 3 was used to make cluster. The cluster is made of 6 beads placed at the corner of the prism. The beads are cemented with acrylic cement at the point of contact and the electrodes were oriented at the pore volume as shown in Figure 3.

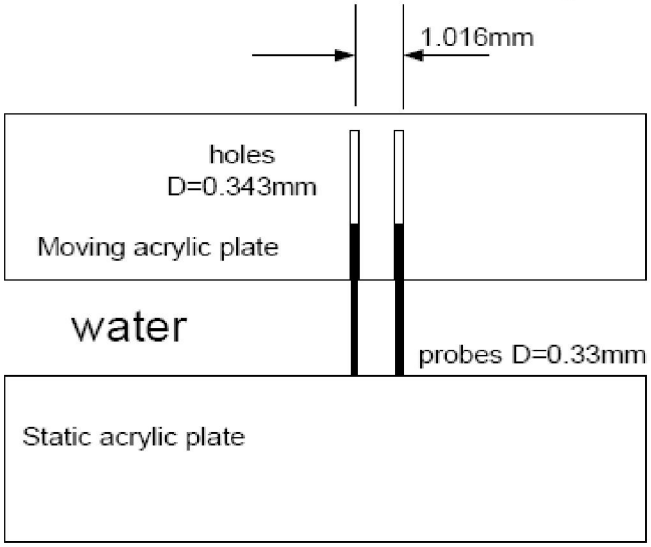

Figure 4 : Schematic of the film thickness probe calibration unit

A calibration system was set up to calibrate the film thickness probe as shown in Figure 4. For this the probes were made on a flat surface with the same electrode size and spacing. The calibration system contained two acrylic plates, one with probes and other one with parallel holes. The holes are such that the probe electrodes can penetrate holes and

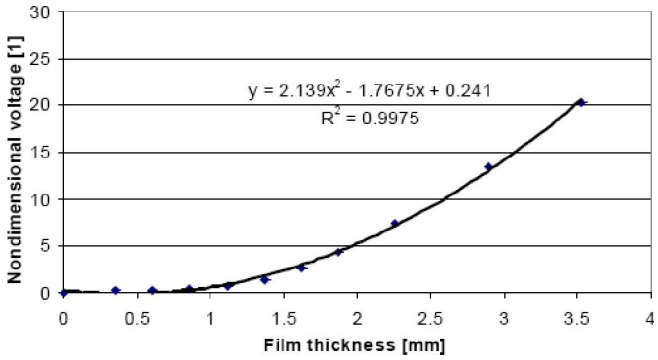

Figure 5 : Calibration data with nondimensional voltage

distance between the plates can be changed to acquire different film thicknesses.

A micrometre screw gage attached to a plate measure the distance between the plates. The thickness tolerance of the acrylic plate was 0.25 mm. The cable was linked to a circuit and the circuit provided the final DC voltage output. Typical calibration curve is shown in Figure 5.

RESULTS OF MEASUREMENTS

Impedance meter void fraction for different flow regime

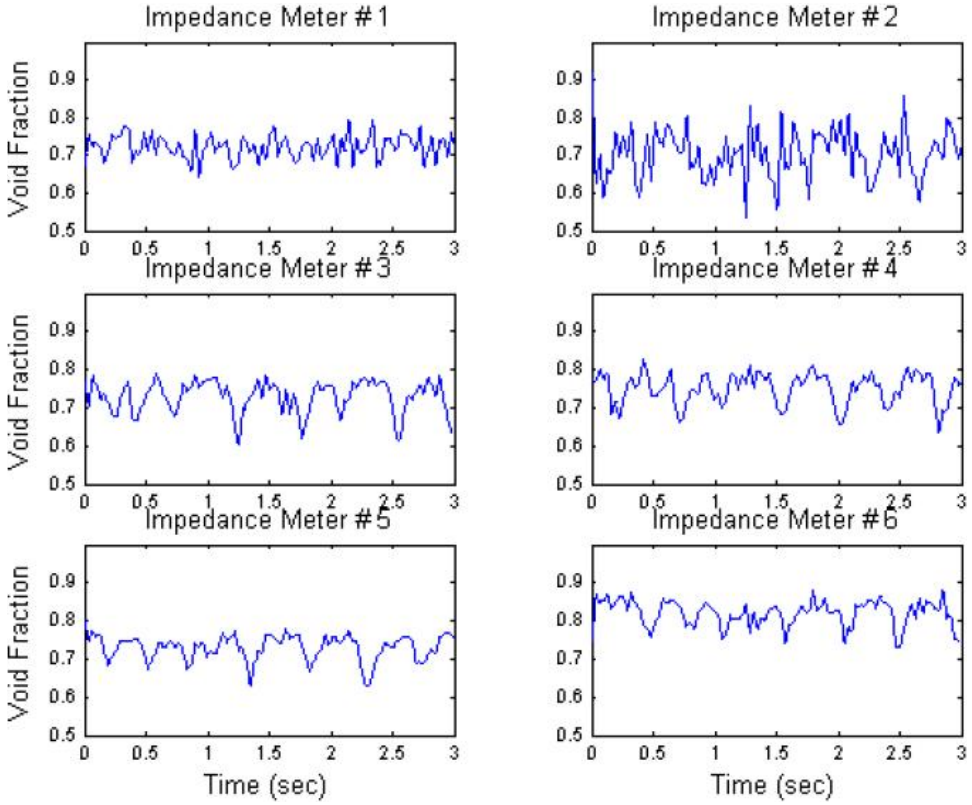

Figure 6 : Impedance meter void fraction time profiles at pulsing flow, U_l =6.7mm/s U_g =1.125m/s

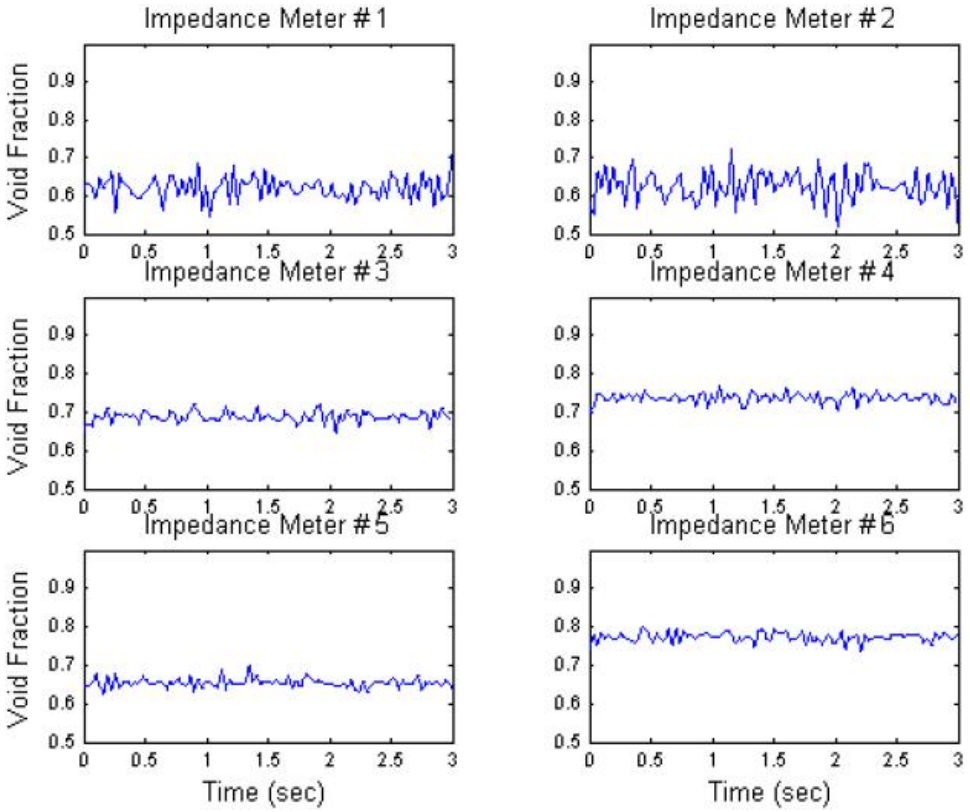

Figure 7 : Void fraction time profiles at trickling flow, Ul =3.4mm/s Ug =8.8cm/s

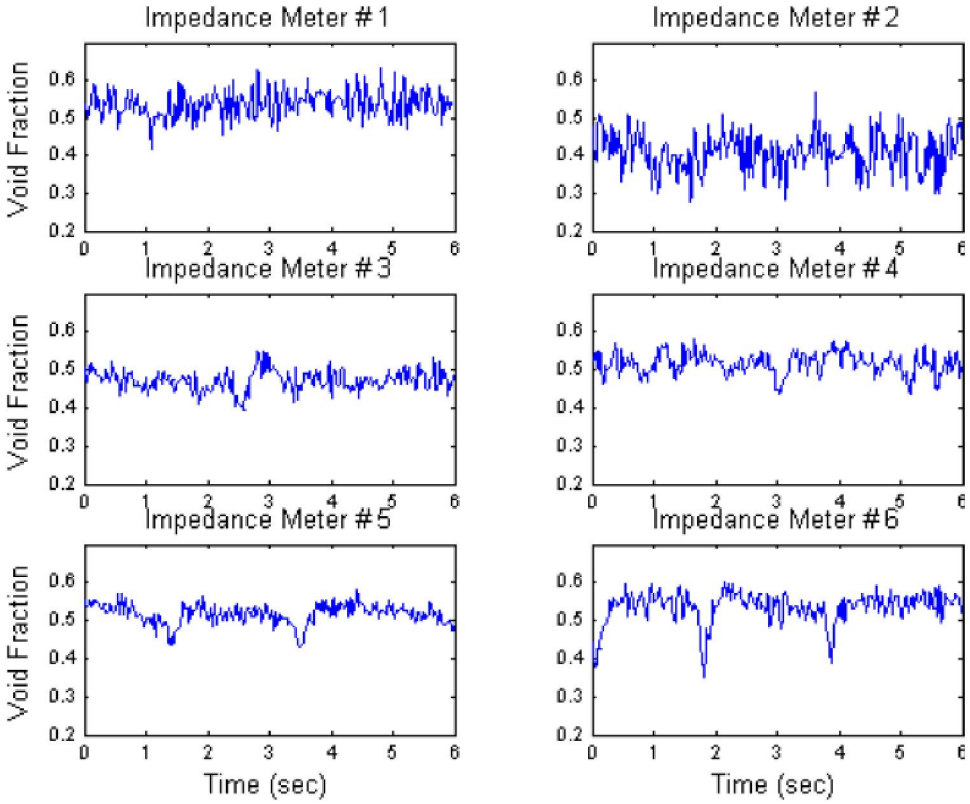

Figure 8 : Void fraction time profiles at transitional flow, Ul =1.2cm/s Ug =0.14m/s

From the signals of impedance meter, void fractions at six different locations along the test section

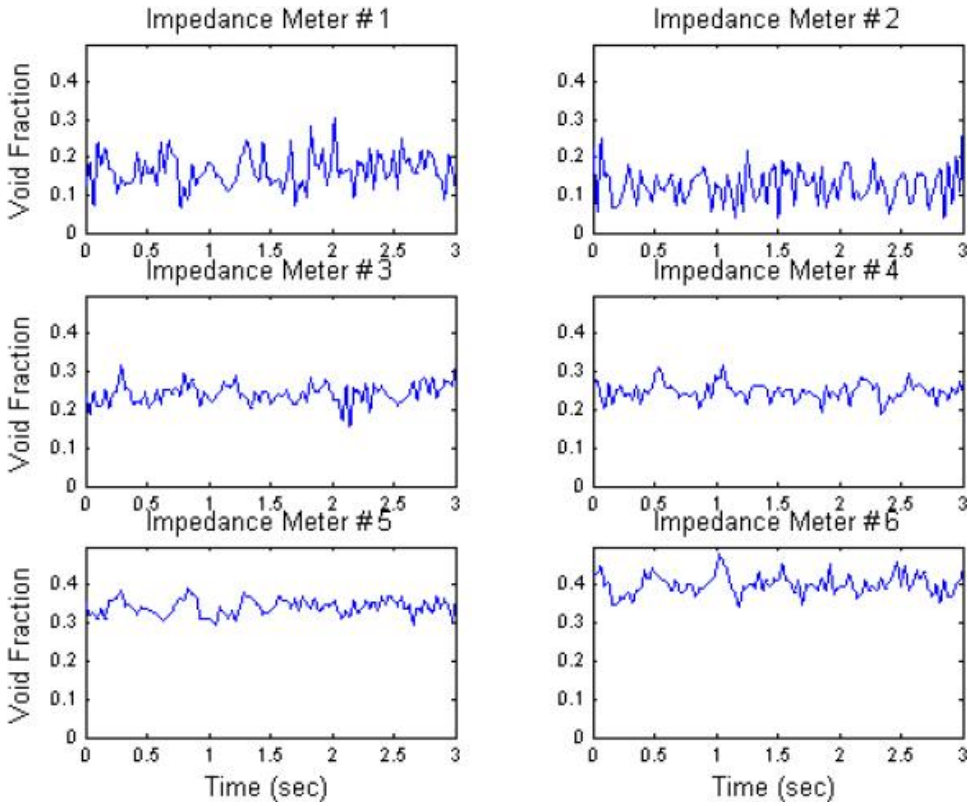

Figure 9 : Void fraction time profiles at bubbly flow, Ul =1.2CM/S Ug =0.14M/S

were recorded. Figure 6 shows the void fraction transient for pulsing flow. Each impedance meter provides a three second profile. Here Ul and Gg are liquid and gas superficial velcoities.

Meters #1, #2, and #6 are measuring two-phase flow under end effect, while similar pulses are displayed in profiles #3, #4, and #5. Output from meter #2 displays greater amplitude of fluctuation than the amplitude of developed pulses at meter #3, #4, and #5. This is because the sudden expansion and contraction of air. The air compressor provides a high pressure at the inlet of the test section. A variety of shapes of pulses are showed in Figure 6. No two pulses show same shape at a certain time and the shape of a pulse is changing while it moves along the test section. Sometimes one pulse breaks apart and sometimes two or more agglomerate to one. The bifurcation of the first pulse shown by probe #4 is an example of such phenomena. The void fraction variance is in a range of 0.2. The difference of average void fractions at various positions can be observed in Figure 6. Changing of void fraction along test section will be discussed in next section.

Figure 7 shows the profiles at trickling flow. Wavy flow has very similar profiles as trickling flow, so they are omitted here. For transitional flow, Figure 8 shows the pulse development clearly.

Bubbly flow void fraction profiles are shown in Figure 5.10. Different from trickling flow, there are still large fluctuations in developed region. This indicates that bubbly flow can be regarded as a type of pulsing flow in which the frequency of pulse is so high that pulse can no longer be discerned. It is possible for the water to flow continuously, but the bubbles are not uniform in the water. They are distributed in a pulse way along test section. As was pointed out in Chapter 3.2, qualitative definition of the flow regimes may not be good enough when data are analysed quantitatively and fuzzy logic application lies in future work.

Axial void fraction distribution

Figure 10 shows the void fraction development along test section at different flow regimes. The pink color square point in figures shows the inlet void fraction in each case. Here wavy flow is omitted as it is similar to trickling flow here. End effects are displayed. Void fraction at meter #2 is always smaller

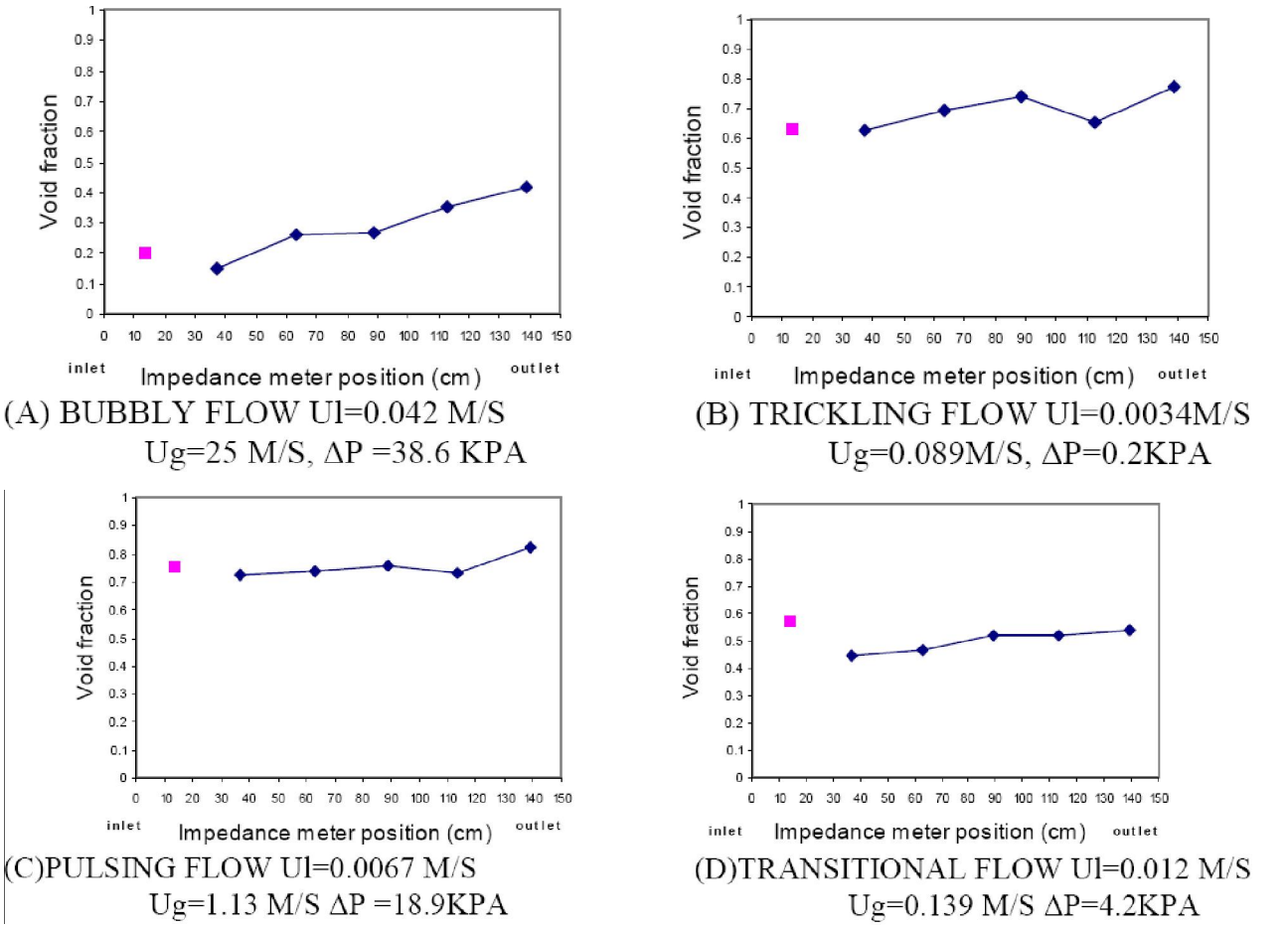

Figure 10 : Void fraction changing along test section at various flow regimes

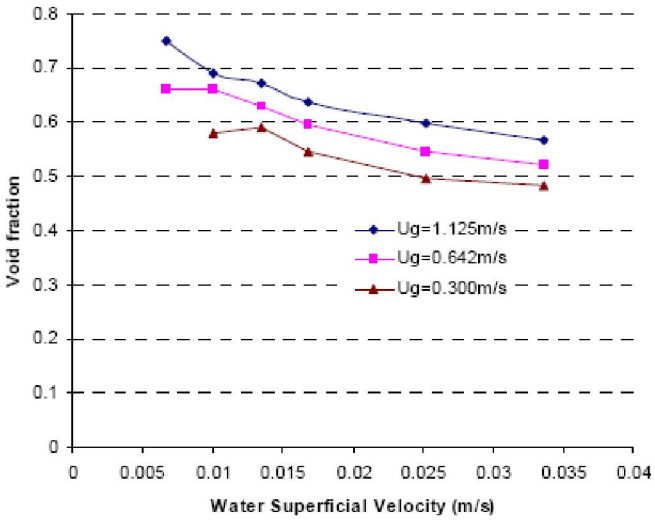

Figure 11 : Void fraction changing with flow rates at pulsing flow

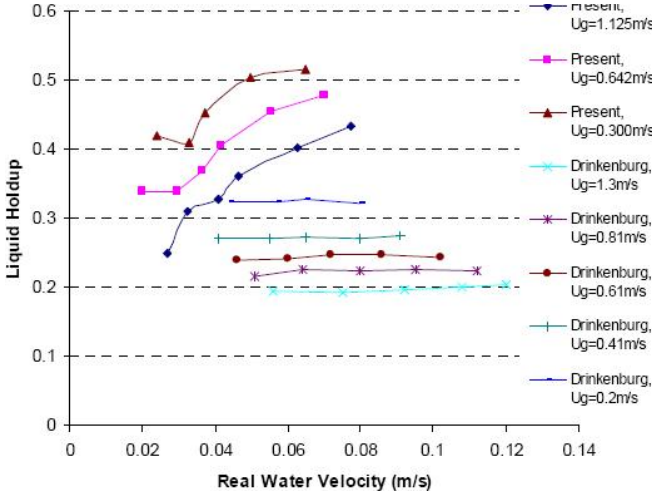

Figure 12 : Comparison of liquid holdup trend with real water velocity, drinkenburg: raschig ring 2.5X2.5MM D=0.05M water/air porosity 0.74; present: sphere 6MM D=0.07M water/air porosity 0.38

than that at meter #1. This proves that usually sudden expansion happens at the position of meter #1 and contraction happens at meter #2.

At outlet, similar process occurs. At trickling flow, air flows continuously and water exerts almost no influence to the air flow, so the air contracts and expands drastically near the outlet. Air expands through the test section. This expansion is significant for high pressure flow, e.g. bubbly flow.

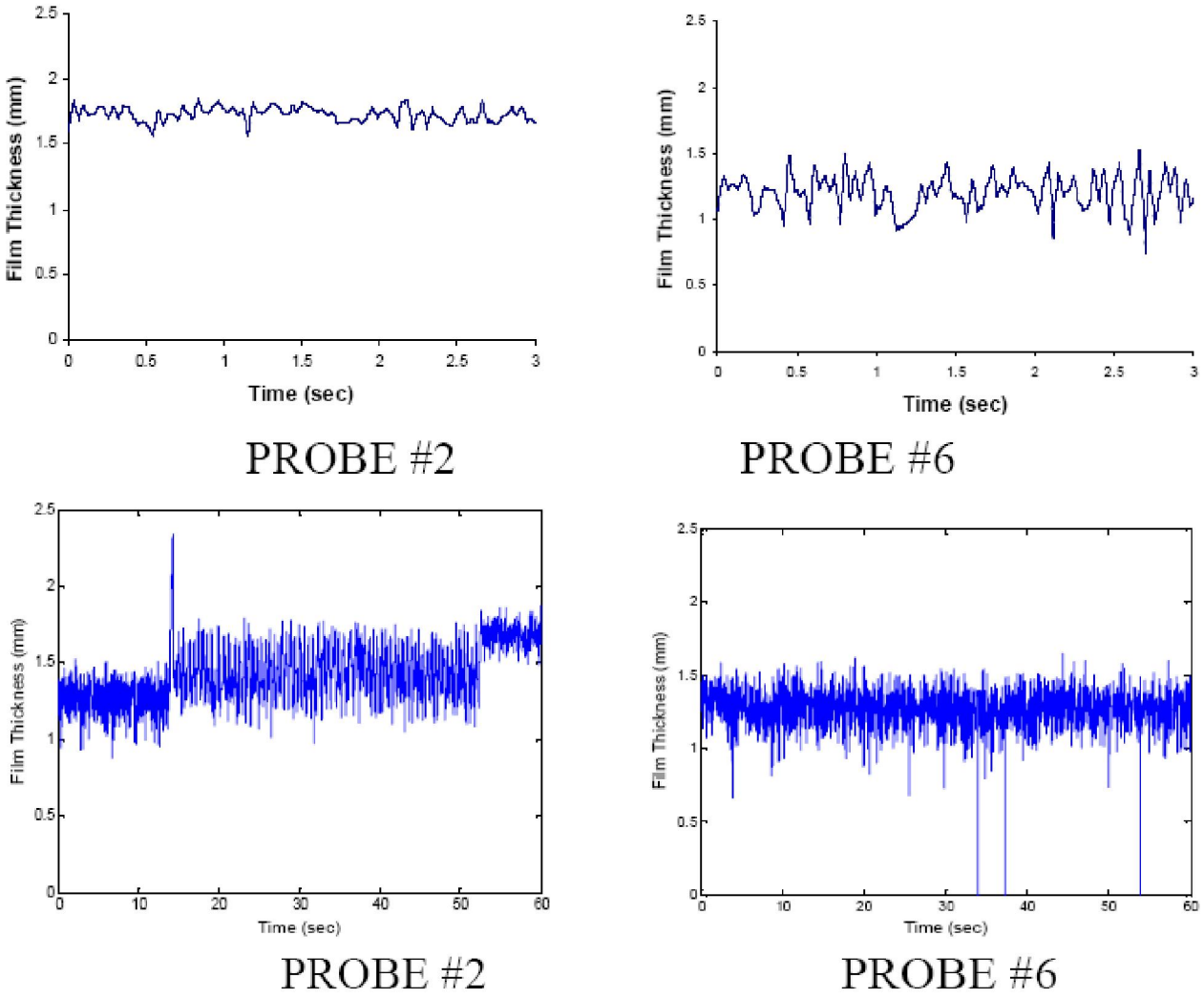

Figure 13 : Film thickness at wavy flow, Ul=0.34 CM/S, Ug=1.05M/S

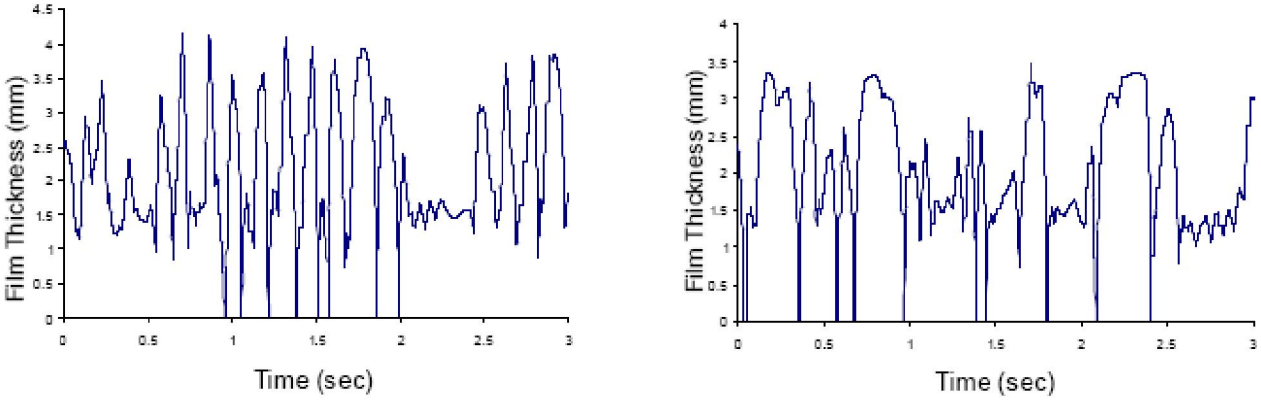

PROBE #6 **PROBE #4**

Figure 14 : Film thickness at transitional flow Ul=1.2 CM/S, Ug=13.8CM/S

Effect of flow on void fraction

For different flow regimes, void fraction changes with flow rates in a different way. Figure 11 displays these changes at pulsing flow. The left points are the beginning points of pulsing flow.

Based on experiment, Drinkenburg et al.,[9] drew the conclusion that liquid holdup keeps constant for varying real liquid velocity during pulsing flow. In

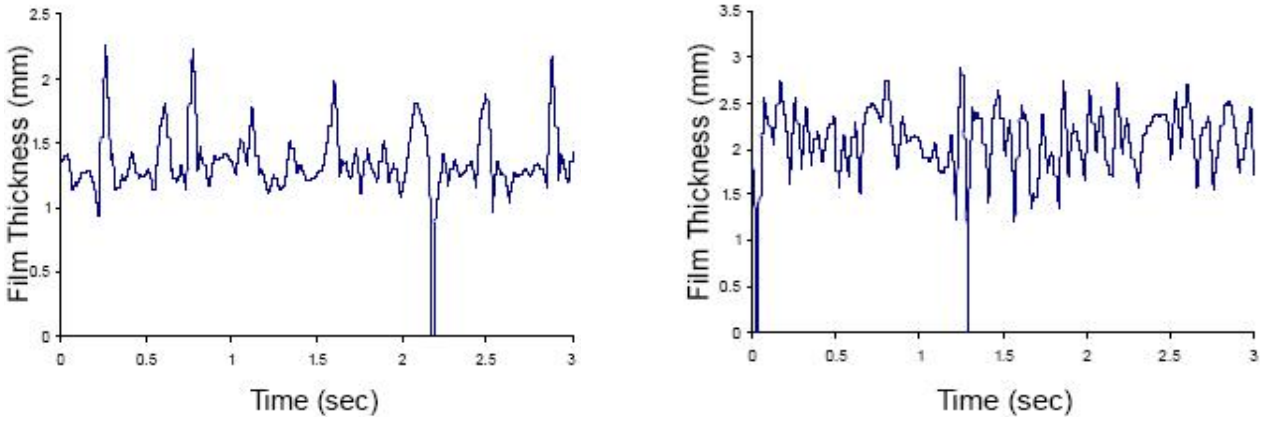

PULSING FLOW, Ul=0.67 CM/S, Ug=1.125M/S, PROBE #4

BUBBLY FLOW, Ul=4.2 CM/S, Ug=0.25M/S, PROBE #4

Figure 15 : Film thickness at pulsing and bubbly flow

his paper, real liquid velocity is defined v as: $v = U_l/\beta$, where β is liquid holdup. This is just a definition and it is different with actual downward liquid velocity by a factor of porosity. Figure 12 shows that there are still increasing trend for liquid holdup to real liquid velocity. Drinkenburg's profiles are also within pulsing flow from the beginning.

The reason for this difference may lie in the significant difference of the packing. Drinkenburg et al.,[9] used Raschig Ring as packing and reached a high porosity of 0.74. They also developed a flow regime model based on their liquid holdup constancy, which may not be applied to low porosity packed bed.

Film thickness

Film thickness probes are used to measure the thickness of liquid on surface, but it does not require the liquid on the surface must be like a film. The images show that water on the packing surface in trickling flows or wavy flow flows like a rivulet, not uniform film. This is because the beads are contacting each other and surface tension pulls water close to the contacting points to remain smallest surface area. Film thickness probes cannot be installed at a very close position to the contacting points because there shape is so highly irregular that calibration will be very complicated, almost impossible. Although disadvantages exist, the film thickness probes in packed bed still bring out credible and important information. Figure 13 shows film thickness at wavy flow.

It was found that vertical probe is better in detecting waves than horizontal probe. This is reasonable since wave at poles should happen more significantly than at equator where wetting area is larger and thickness is smaller. Often water did not run across the equator probes and no wave was detected. In Figure 14, vertical probe #6 shows remarkable thickness fluctuations, while horizontal probe #2 only shows fluctuation at noise level. In trickling flow film thickness at all probes show profiles same as the first figure in Figure 14, so they are omitted here.

At microscopic level, flow at each bead is random and is different with flow at anyone else. The flow changes with time either. The probe #2 figure of the wavy flow film thickness in 60 seconds shows two step changes. The fluctuation amplitude was also changed. The change is random and this figure is not typical; often no step change happens in 60 seconds. The intrusive disadvantage of parallel wire film thickness probe also exerts random influence because surface tension plays a strong role here. For example, the two electrodes may hold some static water when air and water flow rates are very small. So the thickness value is not meaningful, but the changing form displayed by the probes is interesting.

Figure 14 shows the film thickness for transitional flow. At transitional flow regime, there are three different flow patterns for one certain pore channel:

1 Channel may be occluded by water for a short period, e.g. from 2.1 sec to 2.5 sec at probe #4.

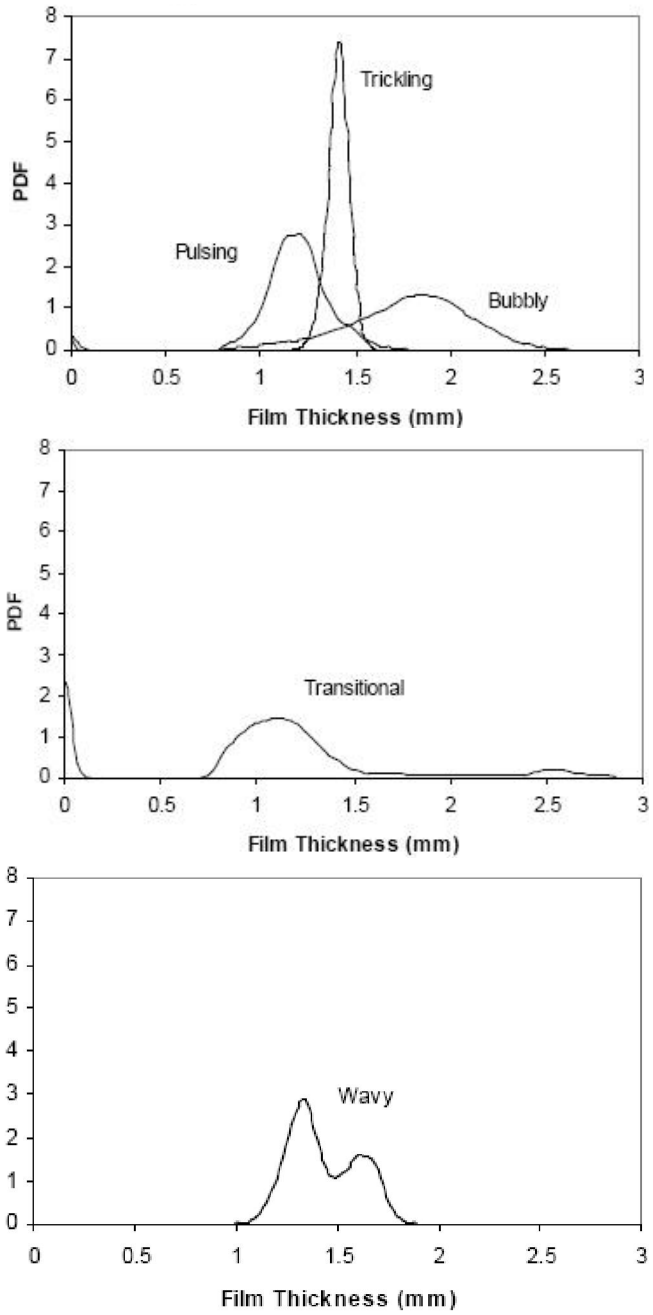

Figure 16 : PDF of film thickness at different flow regimes, probe #2

2 Channel may be open for air flow, e.g., from 2 sec to 2.5 sec at probe #6.

3 Droplets flow continuously across the channel, e.g., from 0.5 sec to 2 sec at probe #6. The droplets are big enough to occlude the channel.

While impedance meters show the pulse development at global level, film thickness probe show the development at pore channel. Now flow is non-uniform across the cross section. Partial pulses happen as embryo of pulses occluding whole cross section.

At pulsing flow, film thickness probes show pulses as well as impedance meter. They display local bubbles during bubbly flow. Figure 15 shows these results:

Film thickness PSF and void fraction PDF

To further process the data, PDF (Probability Density Function) and FFT (Fast Fourier Transform) for the signals were performed. For discrete distributions, the PDF is the probability of observing a particular outcome. It is calculate by following equation[10]:

$$f(y) = \frac{1}{n\lambda}\sum_{i=1}^{n} K\left(\frac{y - y_i}{\lambda}\right) \quad \textbf{(1)}$$

where K is a kernel function, n is the number of equally-spaced points and λ is the bandwidth.

After normalizing above function by dividing it by its integration, PDF, integral of which is one, is obtained. Some symmetric functions can be used as kernel function. For present calculation, normal kernel function was selected:

$$K(t) = \frac{1}{\sqrt{2\pi}}\exp(-t^2/2) \quad \textbf{(2)}$$

Fourier analysis is extremely useful for data analysis, as it breaks down a signal into constituent sinusoids of different frequencies. For sampled vector data, Fourier analysis is performed using the discrete Fourier transform (DFT). The fast Fourier transform (FFT) is an efficient algorithm for computing the DFT of a sequence. It is calculated by:

$$x(n) = \frac{1}{N}\sum_{k=0}^{N-1} x(k)e^{-jk2\pi n/N}, \quad \text{for } n = 0,1,...,N-1 \quad \textbf{(3)}$$

where N is sample number. It corresponds to data taken sample frequency. Corresponding frequency is calculated by:

$$f = n\frac{H}{N} \quad \textbf{(4)}$$

where H is data taken sample frequency.

Figure 16 is the PDF profiles of film thickness at different flow regimes. Flow rates are same as those of previous figures respectively.

Each PDF was calculated from 60 seconds data. For transitional and wavy flow, both single peak

Full Paper

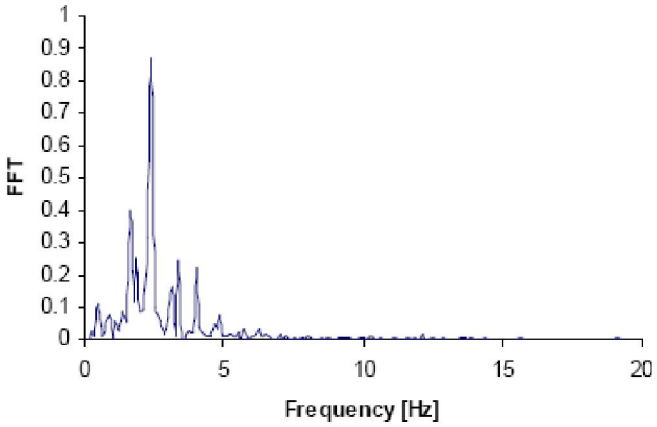

SAMPLE NUMBER: 8000, *H/N*=0.125

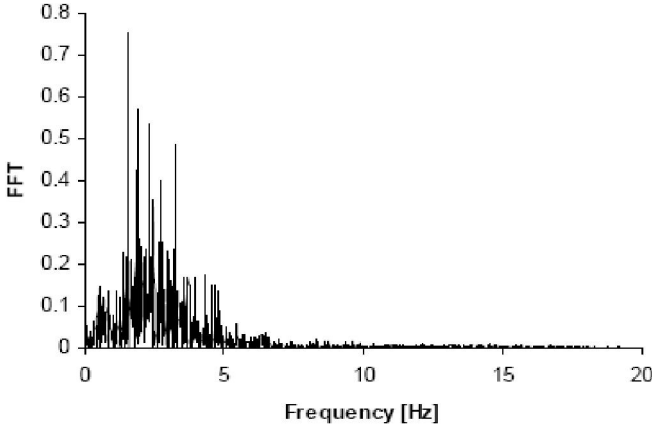

SAMPLE NUMBER: 65536, H/N=0.015

Figure 17 : FFT calculated by dfferent sample numbers

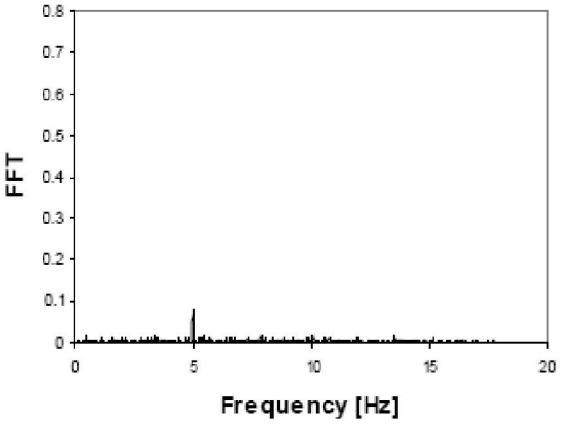

TRICKLING FLOW
Ul =0.34CM/S Ug =8.8CM/S

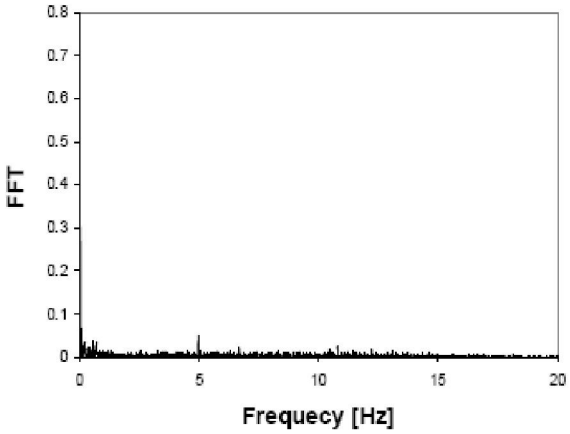

WAVY FLOW
UL=0.34 CM/S, Ug=1.05M/S

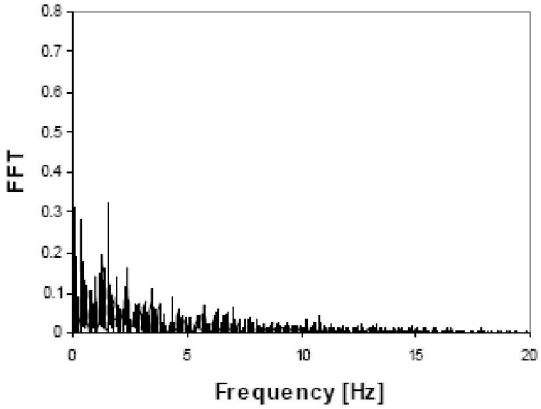

TRANSITIONAL FLOW
Ul =0.34CM/S Ug =8.8CM/S

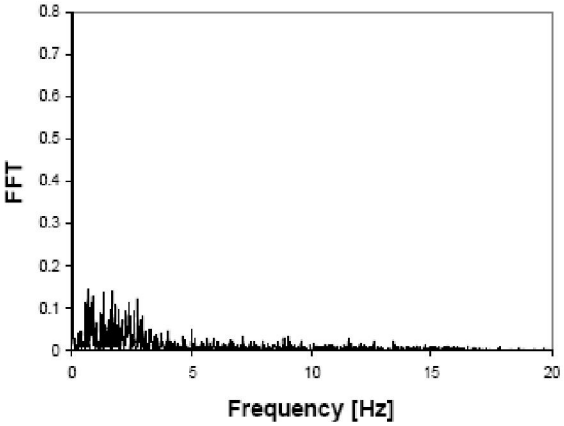

BUBBLY FLOW,
Ul=0.34 CM/S, Ug=1.05M/S

Figure 18 : FFT at different flow regimes

profile and multiple peak profile exist. Here two double peak profiles are shown. But if sample time is long enough, all PDFs at transitional and wavy flow will show multiple peaks. The shape differ-

ence can be applied in flow regime identification. The most probable thickness is not very useful since random factors also influence it. But other parameters, like peak value, width at half peak, and resolution can be used for training and identification in neural network method. PDF of void fraction and differential pressure can also characterize flow regime and be used for flow regime identification.

The FFT result shows a spectral energy distribution on frequency. Different sample numbers give different results, Figure 17 shows a comparison, calculated from void fraction signal for pulsing flow Ul=6.7mm/s Ug=1.125m/s, sampled from impedance meter #5.

The calculation speed is faster when the sample number is 2^n. Our data taken sample frequency is one kilohertz and 60 seconds data were taken, so data taken sample number is 60,000, less than 65536. For such case calculation sample number vector is padded with trailing zeros to full length.

For the original void fraction profile in Figure 6, non-uniform spacing between pulses was observed. The pulses are not running with a strictly

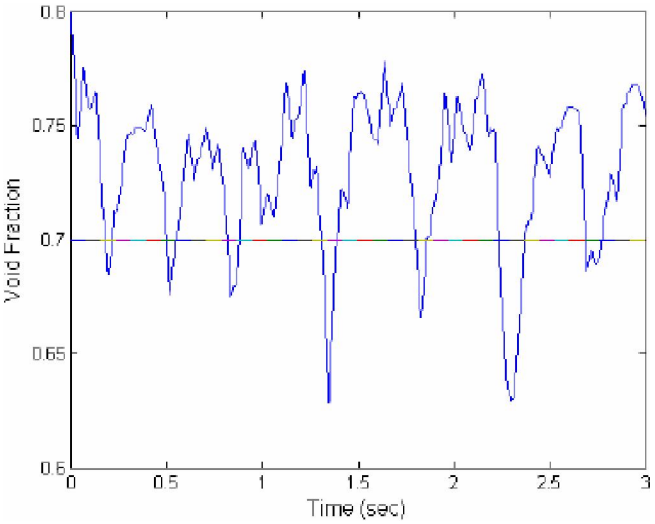

Figure 19 : Pulse count, Ul =6.7MM/S Ug =1.125M/S, from impedance meter #5

uniform frequency. So it is reasonable to characterize wave with multiple frequency. This is shown when sample number is large and accuracy is high (0.015). When a small amount of samples were calculated, accuracy is not good, e.g., when sample number is 8000, the interval between frequencies is 0.125. However, the wave can be characterized to one main frequency approximately. This topic is discussed further in next section.

Figure 18 shows FFT results for other flow regimes, calculated from impedance meter #4 void fraction.

Frequencies extracted from bubbly flow signals also prove that bubbly flow is actually a further development of pulsing flow in which pulse can no longer be discerned. With the characteristics of FFT, PDF and original profiles of void fraction, film thickness and differential pressure, flow regime identification can be realized in a scientific quantitative method.

Hydrodynamic properties of pulses

Pulsing flow through a packed bed is reminiscent of the slug flow in a tube. But pulses in a packed bed bear little hydrodynamic resemblance with slug flow in a tube. In a tube Taylor bubbles and water slugs are clearly separated, the void fraction in the bubble region is almost one, and in the water slug region the void fraction is close to zero. The bubble velocity is exactly equal to the gas velocity and the

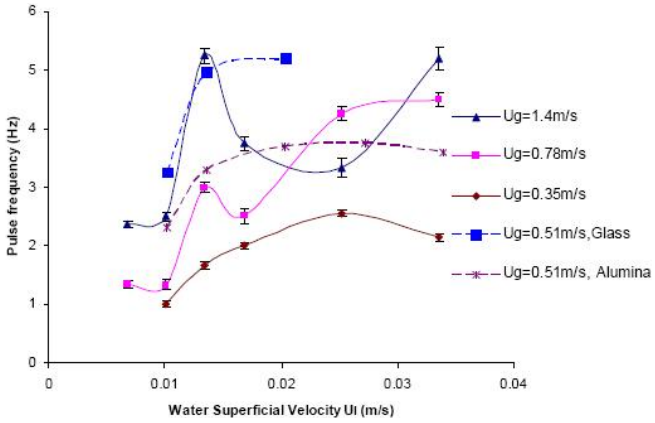

Figure 20 : Pulse frequency

slug velocity is not significantly different from the water velocity. As for pulses in a packed bed, the difference between maximum void fraction and minimum void fraction is around 0.2. The change between maximum and minimum is so smooth that no air region or water region can be identified. The pulse velocity is much higher than the water velocity. A pulse can be described more or less as a wave, taking in fresh liquid at the front and leaving liquid

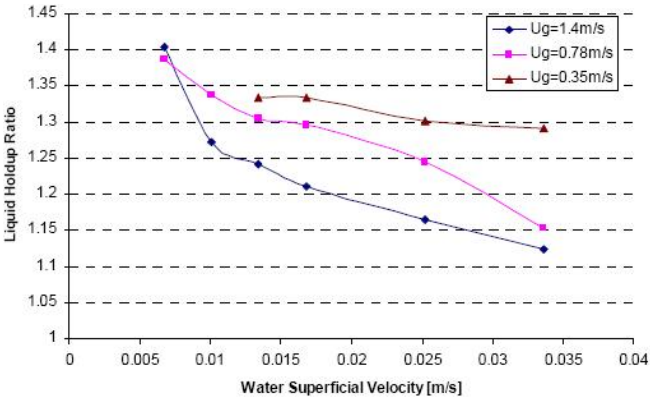

Figure 21 : Ratio of maximum to average liquid holdup

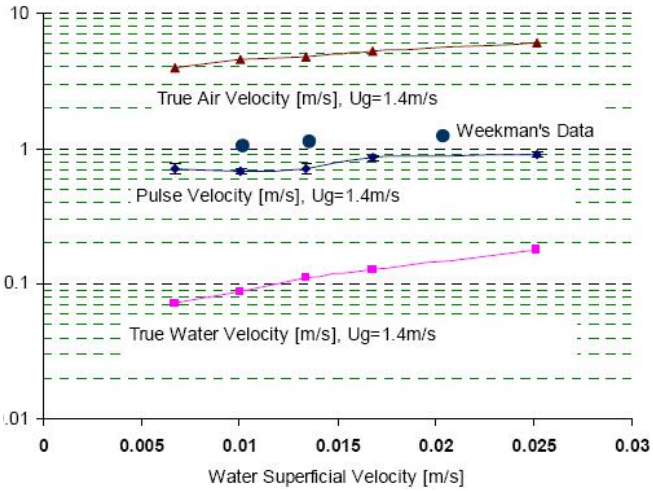

Figure 22 : Pulse velocity, Y axis in M/S

behind at its back. Figure 6 shows pulses in a variety of shapes. High speed camera images show that pulses also change while they flow down the test section. The coalescence of two pulses or the breaking apart of one pulse also occurs. Research into hydrodynamic properties of pulses has a great meaning in chemical engineering since heat and mass transfer is decided by the axial and radial mixing due to the pulses. The artificial induction of natural pulses has been suggested[11].

Pulse frequency

In literature, only a few sets of pulse frequency data for pulsing flow in packed bed were presented. Drinkenburg et al., [9] described two methods for this measurement: microphone and conductivity cell. In the microphone method, a microphone was used to detect noise resulting from pulses. In the other method, a conductivity cell was placed in a separate measuring section downstream of the outlet of the test section. Original voltage signals were processed in a complicated way afterwards. These measurements can offer only one average frequency for the whole test section, assuming frequency development can be neglected. Sato et al.[12,13] and Weekman and John[14] also reported some data on pulse frequencies and pulse velocities.

Based on the small sample number FFT calculation, frequency measurement in pulsing flow is realized. The sample number is set as the largest number which can characterize a single main frequency. Accuracy for such calculation is not good compared with calculations from all samples, but this is due to the non-uniform frequency property of the flow, not from the measurement method. A pulse counting method was also used for comparison. In Figure 19 a criterion was set and pulse number was counted.

Frequency calculated in this method for 60 second data is approximately equal to the frequency from FFT method.

Pulsing flows at higher air-water flow rates are chaotic and the criterion for identifying pulse is difficult to set. Observation from images also cannot provide an accurate count because sometimes it is difficult to determine the pulse identity. The sample number in the FFT method also tends to be smaller and accuracy turn worsens.

Figure 20 shows the pulse frequency changing with flow rates. Weekman and John[14] data were added as dashed lines for comparison. All their data were measured at a gas superficial velocity of 0.51m/s. Upper line corresponds to packing of 5mm diameter glass spheres, porosity 0.39. Lower line is from packing of 6mm diameter alumina spheres, porosity 0.43.

The original data for the three profiles were measured when the air flow rotameter was set as 6 SCFM, 4 SCFM, and 2 SCFM respectively. Since the air pressures at the rotameter are changing along the profiles, true air flow rates rise slightly with the increasing water flow rates while the rotameter shows the same flow rates, so the gas superficial velocities shown in Figure 20 are nominal values. They are middle values of the three superficial gas velocity sequences and errors are within 20%. 9Drinkenburg et al. (1983) drew the conclusion that

only pulse frequency varies significantly with water flow rate. Comparison is omitted here because of the large porosity difference.

Ratio of maximum to average liquid holdup

The extra liquid holdup taken by the liquid pulses can be analysed quantitatively. Ratios of the maximum to average liquid holdup are shown in Figure 21 with varying flow rates. Maximum liquid holdup is the mathematical average of all the maximum liquid holdup values for all the pulses. The maximum from the single largest peak is influenced by some random factors. The maximum liquid hold up was underestimated by the impedance meter. The impedance meters are 8 cm long and the length of the water pulses are usually shorter. The calculated liquid holdup is the volume averaged liquid holdup. The volume contains a column with a diameter of 6.9cm and height of 8cm.

This ratio tends to be smaller for higher air or water flow rates. Most left points are close to transitional region and cannot be considered together with developed pulsing flow. The result is reasonable since high flow rate pulsing flow is close to bubbly flow and axial air-water mixing is better. For Drinkenburg et al.,[9] high porosity packed bed, the ratio of the maximum to minimum liquid hold up is nearly a constant of 1.6.

Pulse velocity

It is difficult to calculate pulse velocity from void fraction or film thickness signals. One certain pulse shown by one certain impedance meter usually corresponds to one pulse shown by the lower impedance meter at a later time point (Figure 6). The pulse velocity is just the spacing of the two impedance meter divided by the time interval. However, no justifiable method has been found to identify the corresponding pulses. The shape of the pulse is changing very fast. It is common for a thin high pulse at a certain impedance meter to develop to a thick short one at the next meter. Coalescence and breaking apart make this more complicated.

Because of this, images from high speed camera are used to calculated pulse speed. Positions of the pulses were traced frame by frame. This means that the pulse moving distance divided by the time interval between frames is the pulse velocity. At each flow condition, ten pulses were traced and the final pulse velocity is the arithmetic average of the ten. Errors shown in Figure 22 are standard deviations. Three data points of pulse velocity from Weekman and John[14] paper were added for comparison. Weekman and John[14] used glass spheres as packing. Diameter is about 5mm and porosity is 0.390. The three points were measured at a gas superficial velocity of 1.13 m/s. Sato et al[12,13] acquired result from experiment data that pulse velocity increases along the test section. That is because the water pulses are blown down by gas flow and gas velocity increases due to its expansion.

For comparison, true water velocity v_f and true air velocity v_g are also shown, which are defined as $v_f = U_l/(\beta\varepsilon)$ and $v_g = Ug/(\alpha\varepsilon)$, where ε is bed porosity and α and β are gas and liquid fraction respectively. Pulses are moving much faster than water. This indicates that pulses are just the appearance of waves, which are blown down by gas flow, without carrying water down. The fact of air moving fast than pulses is also reasonable since water pulses cannot block all channels. For all of the above cases, maximum liquid holdup is less than 0.5, leaving enough space for air to penetrate.

Water cannot fully occupy all the pore channels even at the largest liquid holdup condition, though our film thickness probes cannot show this fact. On the other hand, in Figure 15 the film thickness probe shows a similar pulse density as the impedance meter. It can be expected that the true phenomena happening at a typical pore during a water pulse should be very fast random alternation of water and air occupations since no real boundary exists among pore channels. Because of the stronger surface tension resulting from the intrusive electrodes, the probes keep holding water once pulses come. To overcome this shortcoming, flush mounted film thickness probes should be developed in the future.

CONCLUSIONS

Experiments were conducted in a trickle bed reactor in bubbly, pulse and trickle mode of operation and the flow characteristics were measured with

Full Paper

local film thickness probe and void meter. From film thickness probe signals, three different flow patterns were observed in pores for transitional flow. The impedance meters are proved that they can provide credible data with high responsive speed. FFT and PDF were calculated from original data and different flow regimes show different profile shapes. Frequencies extracted by FFT can characterize the two-phase flow and show some phenomena which cannot be displayed by original signal. Pulse frequency was calculated by the FFT method.

ACKNOWLEDGMENT

The project was partly supported by National Research Foundation of Korea under BK 21 plus program.

REFERENCES

[1] C.N.Satterfield; AIChE J., **21**, 209 **(1975)**.
[2] V.V.Ranade, R.Chaudhari, P.R.Gunjal, Trickle Bed Reactors-Reactor Engineering & Applications, Elsevier B.V. ISBN: 978-0-444-52738-7 **(2001)**.
[3] W.W.Clark; Int.J.Multiphase Flow, **19**, 295 **(2002)**.
[4] K.C.Kang, M.H.Kim; Int.J.Heat Mass Transfer, **18**, 423 **(1992)**.
[5] M.Miya, D.E.Woodmansee, T.J.Hanratty; Chemical Engineering Science, **26**, 191 **(1971)**.
[6] R.C.Brown, P.Andreussi, S.Zanelli; Canadian Journal of Chemical Engineering, **56**, 754 **(1978)**.
[7] J.E.Koskie, I.Mudawar, W.G.Tiederman; Int.J.Multiphase Flow, **15**, 521 **(1989)**.
[8] M.Kim, H.Kang; The development of a flush-wire probe and calibration technique for measuring liquid film thickness, Presented at ASME Winter Annual Meeting, Dallas, FED-99, HTD-155- 31, **(1990)**.
[9] A.A.Drinkenberg, J.R.Blok, J.Varkevisser; Chem.Eng.Sci., **38**, 687 **(1983)**.
[10] A.W.Bowman, A.Azzalini; Applied Smoothing Techniques for Data Analysis', Oxford University Press, **(1997)**.
[11] J.G.Boelhouwer, H.W.Piepers, A.A.H.Drinkerburg; Chemical Engineering Science, **57**, 3387 **(2002)**.
[12] Y.Sato, T.Hirose; 1973a, J.Chem.Eng.Jpn., **6**, 147 **(1973)**.
[13] Y.Sato, T.Hirose; 1973b, J.Chem.Eng.Jpn., **6**, 315 **(1973)**.
[14] V.W.Weekman Jr., E.M.John, AIChE J., **10**, 951 **(1964)**.